

# Multiband responses in high- $T_c$ cuprate superconductors

G. Nikšić,<sup>1</sup> I. Kupčić,<sup>1</sup> O. S. Barišić,<sup>2</sup> D. K. Sunko,<sup>1,\*</sup> and S. Barišić<sup>1</sup>

<sup>1</sup>*Department of Physics, Faculty of Science, University of Zagreb,  
Bijenička cesta 32, HR-10000 Zagreb, Croatia.*

<sup>2</sup>*Institute of Physics,  
Bijenička cesta 54, HR-10000 Zagreb, Croatia.*

We report on the interplay of localized and extended degrees of freedom in the metallic state of high-temperature superconductors in a multiband setting. Various ways in which the bare magnetic response may become incommensurate are measured against both phenomenological and theoretical requirements. In particular, the pseudogap temperature is typically much higher than the incommensurability temperature. When microscopic strong-coupling effects with real-time dynamics between copper and oxygen sites are included, they tend to restore commensurability. Quantum transport equations for low-dimensional multiband electronic systems are used to explain the linear doping dependence of the dc conductivity and the doping and temperature dependence of the Hall number in the underdoped LSCO compounds. Coulomb effects of dopants are inferred from the doping evolution of the Hartree-Fock model parameters.

**Key words:** Emery model, magnetic fluctuations, electron-doped superconductors.

**Running title:** Multiband responses in high- $T_c$  cuprates

## 1. INTRODUCTION

The mechanism of high-temperature superconductivity (SC) in cuprate perovskites remains the pre-eminent open problem of solid-state physics today, more than 25 years after their discovery. A common paradigm of these materials emphasizes the strong on-site Coulomb repulsion  $U$  (“large  $U$ ”) on the copper sites, based on the ubiquitous insulating antiferromagnetic (AF) phase of the parent compounds, eventually replaced by the SC phase of the metallic doped materials. It begs the question, whether the interesting SC part of the phase diagram is better described starting from a metal, or from an insulator. A large body of evidence indicates that the metallized materials themselves suffer a crossover between the “deeply” underdoped (conducting without SC) and “ordinary” underdoped (suboptimally SC) regimes, most obviously in the temperature dependence of the normal-state conductivity, which changes from an insulating-like upturn, but with finite residual resistivity, to a downturn interrupted by SC, around 6% doping e.g. in LSCO [1]. It is also visible in ARPES [2] as the smoothing out of a fairly discontinuous Fermi-surface (FS) gap (U-shaped gap) towards a d-wave form (V-shaped gap). In the normal state, one can see the ARPES intensity around the nodal point, the so-called FS arc, stretch out towards the zone boundary as optimal doping is approached.

The unifying theme of this article is that the arc metal behaves essentially as a Fermi liquid, with two important qualifications. First, the spectral weight of the conducting states is less than unity, and depends on doping: the carriers spend part of their time in localized states, because of the large  $U$ . Second, the metal cannot be properly described in an effective-mass approximation, because (a) the pseudogap (PG) scale appears in the low-energy responses, and (b) the Fermi velocity varies significantly along the arc. Such a simple understanding of the low-temperature metallic state is contingent, however, on a multi-band approach, in which the chemical composition of the copper-oxygen conducting plane plays an important physical role.

## 2. MAGNETIC RESPONSES

### 2.1. The high-temperature approach

A nearly-universal feature of the underdoped cuprates is an incommensurate magnetic response, near the AF wave-vector, observed in neutron scattering [3–5]. The incommensurability is collinear for the underdoped (SC) materials

---

\*Electronic address: dks@phy.hr

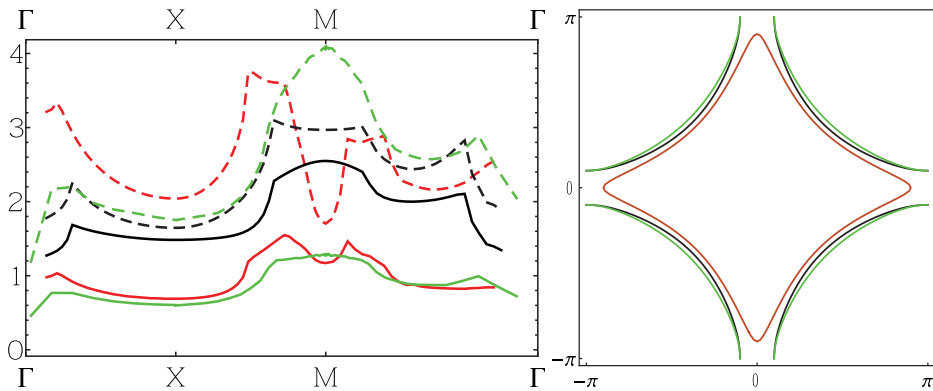


FIG. 1: Left: free susceptibilities in the three-band model (broken lines), and with the band-fermion legs renormalized to first order (full lines), as described in the text. The corresponding Fermi surfaces are shown at right. The two similar open Fermi surfaces differ in the ratio  $|t_{pp}/t_{pd}|$ , which is larger for the one with an incommensurate bare response.

and diagonal for the deeply-underdoped (non-SC) compositions. When it is collinear, it also changes to diagonal at large energy-transfer (frequency).

The usual approach [6, 7] to modelling such a response in a metal is to look for an incommensurability in the high-temperature bare particle-hole (*ph*) susceptibility  $\chi_{\xi\xi'}$  in the appropriate excitation channels  $\xi$ . The general structure of such a susceptibility is [8]

$$\chi_{\xi\xi'} = \chi_{\xi\xi'}^0 + \frac{\chi_{\xi\alpha}^0 U_{\text{eff}} \chi_{\alpha\xi'}^0}{1 - U_{\text{eff}} \chi_{\alpha\alpha}^0}, \quad (1)$$

where  $\alpha$  is the internal degree of freedom presumed to give the incommensurate response, probed by creating and destroying particles in the state  $\xi$ , and with an effective self-interaction (square vertex)  $U_{\text{eff}}$ , discussed below. For the copper-oxide planes,  $\alpha$  are the metallic band states projected onto the copper *d*-orbitals. The high-temperature response can itself be already symmetry-broken [9], or bare with renormalized band parameters (HF) [7].

Our principal result is that the HF response  $\chi_{\alpha\alpha}^0$  changes qualitatively when the strong on-site repulsion is taken into account dynamically, i.e. without any mean-field approximation. Without the on-site repulsion, regimes can be found for both closed and open Fermi surfaces, where the responses  $\chi_{\alpha\alpha}^0$  are incommensurate. They are shown by broken lines in Fig. 1. Full lines show the corresponding responses  $\chi_{\alpha\alpha}^1$ , which include a first-order renormalization of the metallic band fermions, taking into account the on-site repulsion. Only the response of the closed (around  $\Gamma$ ) FS remains incommensurate, while all the open-FS responses are now commensurate.

The large  $U$  is infinite in this approach [8]. The low-energy scales are generated by a waiting effect, where the metallic hole must wait for the copper site to be free before visiting it, which creates a scattering vertex between the hybridized holes in the band. In the low-energy limit, this gives rise to a constant  $U_{\text{eff}} \approx t_{pd}^4/(\varepsilon_d - \mu)^3 \equiv U_{d\mu}$ , to be compared with the usual charge-transfer  $J$ , where the empty oxygen orbital energy  $\varepsilon_p$  appears instead of the band chemical potential  $\mu$ , leading to similar numerical scales,  $U_{d\mu} \sim J$ , despite the profoundly different physics. Mean-field approaches miss the waiting effect, because they are by construction only able to renormalize the band parameters, allowing for qualitatively the same high-temperature incommensurability as in the non-interacting system, shown by broken lines in the figure. By contrast, the waiting effect redistributes the spectral strength of the particle-hole excitations in the Brillouin zone, leading to a qualitatively different, commensurate susceptibility.

It is also possible to get incommensurability in  $\chi_{\xi\xi}$  directly from the first term,  $\chi_{\xi\xi}^0$ , by choosing the  $\xi$  channel to probe the oxygen sites, however the response is typically much smaller than  $\chi_{\alpha\alpha}^1$ , so it would be quite unnatural to try fine-tuning the parameters so that the non-interacting term should dominate the interacting one. Finally, incommensurate responses may appear close enough to half-filling on both doping sides when  $|t_{pp}/t_{pd}| \ll 1$ , because the system reverts to particle-hole symmetry [10]. That is not a realistic physical regime for the cuprates, in which particle-hole symmetry is strongly broken.

The common vein of the standard approaches outlined above is that one gets the incommensurate response already in the high-temperature phase, which then triggers an incommensurate low-temperature response through the denominator in Eq. (1), at the same wave-vector. Measurements show, however, that the response is incommensurate at temperatures still above the SC  $T_c$ , but considerably below the pseudogap  $T^*$ , which is the natural candidate for the transition temperature in this context. Around  $T^*$  it is still commensurate, as our strong-coupling calculation suggests it should be. Therefore we take the transition from high-temperature to be the commensurate one, and investigate the so-obtained low-temperature phase in the following.

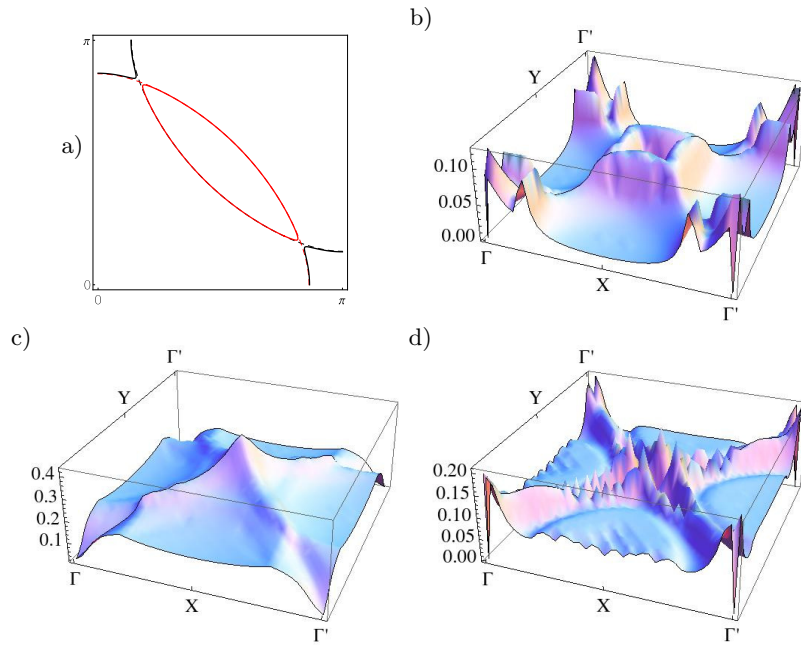


FIG. 2: a) FS reconstructed from two subbands, showing a nodal and antinodal part. b) Intraband antinodal response. c) Interband nodal-antinodal response. d) Intraband nodal response.

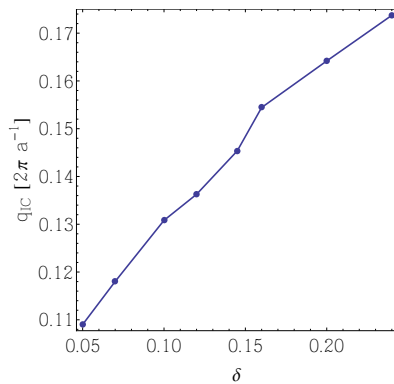


FIG. 3: Dependence of the collinear incommensurability away from AF on the doping, for the free intraband arc response.

## 2.2. The low-temperature approach

While our high-temperature calculation was fully microscopic in its one critical feature — the restoration of commensurability by the dynamical waiting effect — the low-temperature approach is phenomenological. We simply insert the FS gap observed in ARPES into the band dispersion, and calculate the responses of the emerging subbands. The experimental pseudogap is thus mimicked by a true, but  $k$ -dependent, gap. Furthermore, the quasiparticles with gapped dispersion are non-interacting. Both are standard features of zeroth-order low-temperature calculations. We are interested in the bare responses of the reconstructed FS, obtained at a given chemical potential.

Fig. 2 shows the principal responses with a small constant gap, used for pedagogical purposes. The chemical potential cuts across both subbands, producing the well-known disconnected reconstructed FS. The intraband nodal response, which is the response of the arc metal, is collinearly incommensurate, with needle-like peak shapes, consistent with experiment.

Our main physical point is that the other two responses are gapped out in real underdoped materials. They involve the antinodal segments of the FS, which do not contribute when the observed U-shaped gap is inserted. Thus only the nodal (arc) response survives. The doping dependence of its incommensurability is shown in Fig. 3. In a wide range of doping, it follows the experimental rule of thumb  $q_{IC} \propto x$ , where  $q_{IC}$  is the incommensurability away from AF, while  $x$  is the hole concentration away from half-filling, i.e. Ba or Sr concentration in  $\text{La}_2\text{CuO}_4$ . On the other hand, it

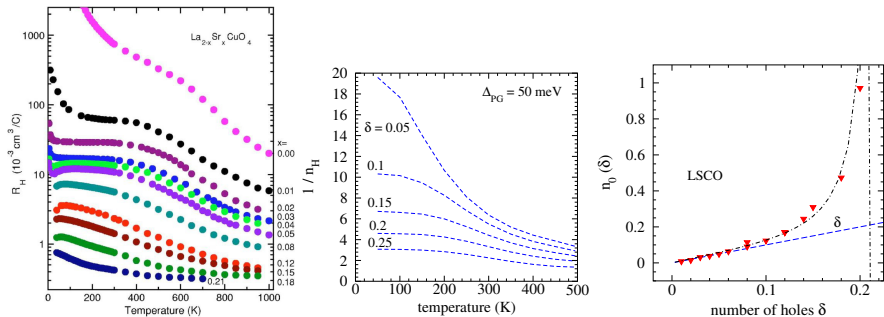


FIG. 4: Left: Measured Hall coefficient  $R_H = 1/(ecn_H)$  in LSCO [15]. Center: Eq. (2). Right: the FS contribution  $n_0(\delta)$ .

is fairly independent of gap size  $\Delta$  as soon as the gap exceeds the temperature, which means it becomes temperature independent as soon as  $\Delta > kT$ . Both the strong doping and weak temperature dependence are consistent with experiment.

The collinear incommensurate responses have thus been identified as the free response of the low-temperature nodal metal. The band composition has been crucial to arrive at this interpretation, because it underlies the microscopic scattering which pushes the high-temperature (strongly interacting) response to commensurability, as the copper-oxygen-hybridized holes scatter on the copper sites. The incommensurate response of the low-temperature arc quasiparticles is experimentally not strong enough to trigger a transition in turn, otherwise the arc would not be conducting in the normal state. This is consistent with our treating them as non-interacting.

### 2.3. The central peak

The calculated high-temperature commensurate response which triggers the transition is not dispersive for energies  $\omega \ll kT$ . This indicates that the transition does not proceed by a Kohn-like anomaly in the paramagnon spectrum, but by a central peak. Such a central peak has just been reported by J. Tranquada at this conference [11], as “gapless magnetic excitations.” It appears [11] that such a peak has been noticed in earlier work, where it was interpreted as a gap with unexpected behavior, becoming smaller with underdoping [12]. We note that Fig. 2 of Ref. [12] shows that the magnetic field dependence of elastic and inelastic neutron scattering is the same for small energy transfers  $\omega < 1.5$  meV, meaning that the width of the central peak is about 15 K.

## 3. ARC CONDUCTIVITY

The low-temperature quasiparticles invoked in the explanation of the magnetic responses are not really non-interacting. Their residual interactions create a pseudogap instead of the true gap used above, which means that the quasiparticle scattering contribution to the resistivity is large, and has indeed the expected Fermi-liquid  $T^2$  dependence in the single-plane mercury and underdoped YBCO compounds. The pseudogap scale  $\Delta_{PG}$  is visible in the temperature dependence of the Hall number  $n_H = 1/(ecR_H)$  as an activation term [13–15],

$$n_H = \frac{n_{xx}^{\text{eff}} n_{yy}^{\text{eff}}}{n_{xy}^{\text{eff}}} \approx n_0(\delta) + n_1 e^{-\beta \Delta_{PG}(\delta)} + \dots \quad (2)$$

which reproduces the rapid falling-off of the Hall coefficient, as shown in Fig. 4. To reproduce the doping dependence, one also needs to take into account that the effective Hall number diverges when  $n_{xy}^{\text{eff}}$ , which is like a net curvature of the Fermi surface, crosses zero. This crossing point is sufficiently close to the physical dopings that the term  $n_0(\delta)$  is strongly non-linear, as also shown in the figure.

Neither of the above effects can be understood from an effective-mass point of view. The effective mass tensor

$$\left( \frac{m}{m^*} \right)_{\alpha\beta}^L = \frac{m}{\hbar^2} \frac{\partial^2 \varepsilon_L}{\partial k_\alpha \partial k_\beta} \quad (3)$$

does not naturally appear in the full quantum expression for the diagonal effective number,

$$n_{\alpha\alpha}^{\text{eff}} = -\frac{m}{V} \sum_{L\mathbf{k}\sigma} [v_\alpha^L(\mathbf{k})]^2 \frac{\partial f_L(\mathbf{k})}{\partial \varepsilon_L(\mathbf{k})}, \quad (4)$$

where  $v_\alpha^L(\mathbf{k})$  is the carrier group velocity, and  $\partial f/\partial \varepsilon_L$  is peaked at the FS, correctly suppressing contributions from carriers deep below it. True, this expression can be formally manipulated to give a Drude-like form, which appears to sum contributions from all carriers,

$$n_{\alpha\alpha}^{\text{eff}} = \frac{1}{V} \sum_{L\mathbf{k}\sigma} \left( \frac{m}{m^*} \right)_{\alpha\alpha}^L f_L(\mathbf{k}), \quad (5)$$

but this only makes sense at the bottom of the band, where the non-diagonal term  $n_{xy}^{\text{eff}}$  in the denominator, which has no effective-mass interpretation, is quiescent. In the cuprates, which are near half-filling, the “non-Fermi liquid” nature of the carriers observed in Fig. 4 is primarily due to the failure of this effective-mass semiclassical limit, not of the Fermi liquid concept itself. On the other hand, the Hall number calculated in this simple band picture needs to be divided by about 4 in order to reproduce the absolute values of the conductivities. This is a strong-coupling effect, by which the mobile carriers spend a large amount of time in localized states, because of the waiting induced by the infinite  $U$ , as explained above. However, the factor of four is not a direct measure of the size of the strong-coupling effect. A careful analysis shows that the strong-coupling renormalization factors generally appear squared, so that a rough estimate of the localized component is rather one-half, further subject to parameter regimes in the three-band model, which distribute the charge between copper and oxygen.

#### 4. IONICITY VS. COVALENCY

The success of the quantum Fermi liquid is qualified by the important limitation, that the doped holes spend only part of their time conducting, and the rest in localized states. Technically, the quasiparticle weight is not fully unity. Physically, bonding in every real material is on a continuous scale between the ionic and covalent limits, and the idea that some orbitals are exclusively localized, while others are exclusively conducting, is an idealization, valid perhaps for the first-column metals, but certainly not for doped transition-metal oxides. Effects of the ionic background in the metallic behavior are the true “strong-coupling” effects in the cuprates. These are, however, least visible at the FS itself, if the latter is simply defined as the point where some intensity is cut off by the chemical potential, because the crossing point in the zone may differ very little from the one in the corresponding non-interacting FS, even if the intensity profile (EDC) is quite different than that of a quasiparticle. Such an “experimentally defined” FS therefore provides a useful insight into the large background scales which define the effective tight-binding parameters.

##### 4.1. Ionic effects on the site energies

An early question in high-T<sub>c</sub> cuprates was how the dopand charge ended in the plane [16]. One possible mechanism is covalent, by which it is discharged into the plane as if by a conducting wire. The other, advocated in Ref. [16], is ionic, by which it affects the chemical balance in the plane by Coulomb fields, so that the plane moves from the ionic to the covalent limit, effectively self-doping. In the tight-binding model, this is reflected as a change in the site-energy splittings, which gives a simple explanation, why the evolution of the FS with doping cannot be fitted with rigid bands.

Typically, hole dopants are introduced into the cuprates in one of two ways. One is to replace the out-of-plane metal anions, as in LSCO, where Sr replaces La. The alternative is to introduce oxygens into interstitial positions, which are presumably cationic, like the stoichiometric oxygens. As an elementary test of the doping mechanism, we investigate Hartree-Fock (HF) band fits to the FS series in LSCO and single-plane Bi2201. We use a four-band model, in which a copper 4s orbital is added to the usual three bands, because that is the minimal model with chemically realistic parameter ranges; further down-folding to the three-band model requires artificially large values of the oxygen-oxygen hopping  $t_{pp}$  [17].

Fig. 5 shows the Fermi-surface fits achieved in the model. Parameter evolution has been constrained principally to the energy of the copper 4s-orbital. A further constraint was to fit the measured positions of the absolute chemical potential within each species. This could also be achieved at all dopings by varying only the 4s level energy, except around 15% doping, where a small increase in the copper-oxygen overlap  $t_{pd}$  was required.

The parameter evolution is summarized in Fig. 6. The most robust finding is that the change of the 4s-orbital energy is in the opposite direction for the two classes of materials. This is simply interpreted as reflecting the different ionic positions of the dopants, supporting in turn the ionic doping mechanism. The large overall variation of  $\varepsilon_s$  is due to the fact that it is the only parameter varied, while the comparatively small non-uniformity in  $t_{pd}$  cannot be interpreted at this level of analysis, because other similarly small scales, such as the kink scale, are not included. Notably, the 4s-orbital energy is the only site energy whose variation alone can account for the whole FS evolution

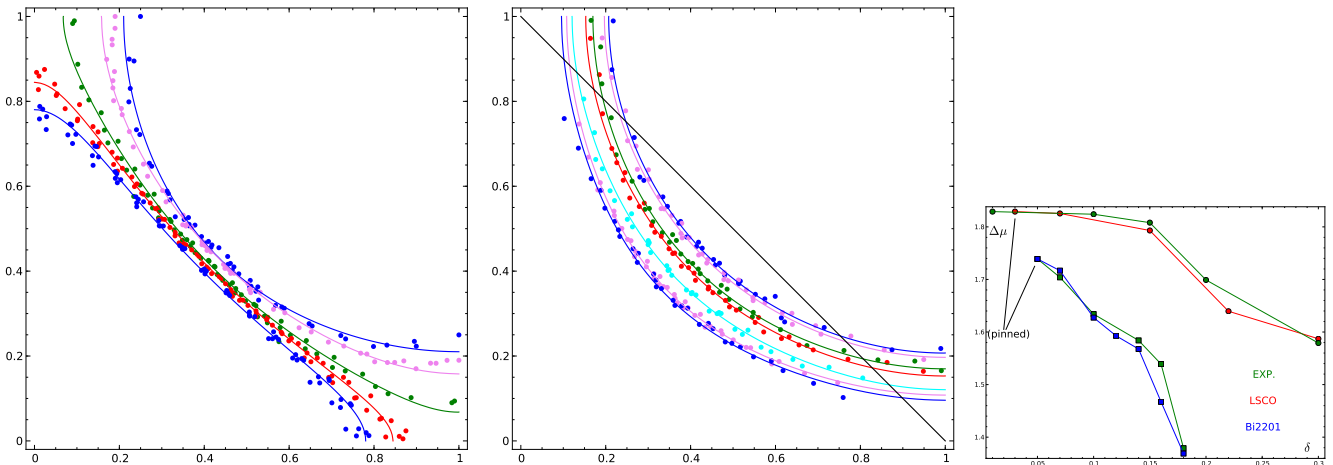


FIG. 5: FS fits with a four-band model for LSCO (left), Bi2201 (center), and the corresponding chemical potentials (right). The calculated chemical potentials have been shifted (“pinned”) to their measured values at lowest doping.

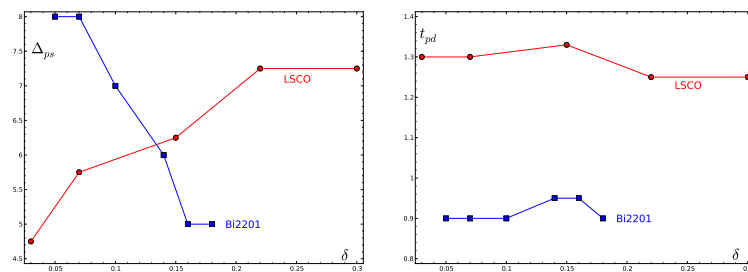


FIG. 6: Parameter evolution in the four-band model corresponding to the fits in Fig. 5. All other parameters are kept fixed.

and observed chemical potential shift in both materials. The *increase* in the splittings  $\Delta_{ps}$  and  $\Delta_{ds}$  with doping in LSCO accounts for the peculiar hockey-stick shaped shift in the chemical potential, and its overall smaller range than in Bi2201, because the rigid-band-filling trend of the chemical potential runs counter to the trend determined by the increase of the level splittings. In the interstitially doped Bi2201, both trends are in the same direction.

#### 4.2. Ionic effects on extended states

Violations of the Luttinger sum rule have been observed [18] in the experimental FS crossings of the previous section. They are small relative to the experimentally defined FS, and for the reasons outlined above, such a small shift is presumably influenced by any number of interacting scales, large and small. Nevertheless, an important qualitative trend is observed in the data, namely that the violations change sign, from under- to over-compensated, at around 10–15% doping.

The same strong-coupling theoretical framework as for the magnetic responses can describe violations from the Luttinger rule. The scattering of the band states induces a transfer of spectral weight into incoherent localized states on the copper sites, away from the Fermi energy. With doping, there is both a redistribution between localized and itinerant states, and between the copper and oxygen orbitals. The latter also affects the overall weight of the states, because the blocking by the infinite  $U$  removes some states to infinity as the copper level is filled. In a wide range of parameters, the net effect is a change in sign of the Luttinger-rule violation roughly, and robustly, where it is observed experimentally, as shown in Fig. 7. We conclude that the dominant mechanism of Luttinger-rule violation is by the large- $U$  removal of spectral weight away from the Fermi level, with quantitative details left to be explained by the lower-energy mechanisms, such as the nodal kink, not included in the calculations depicted in the figure.

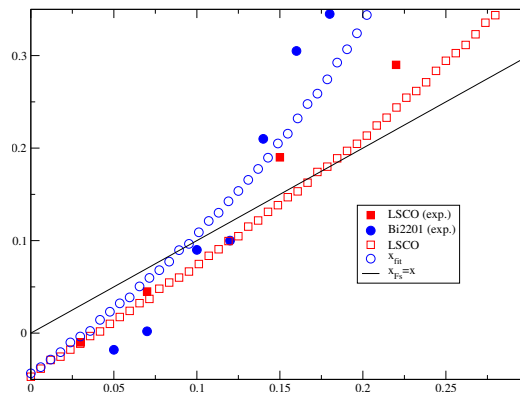


FIG. 7: Violations of the Luttinger sum rule.

## 5. CONCLUSION

The cuprates lie in a crossover region between the ionic and covalent limits. The ionic aspect is reflected by the doping affecting the underlying tight-binding parameters of the metal directly, in addition to changing the concentration. Close to the Fermi surface, however, there is every indication that the metal behaves as a Fermi liquid out of a reconstructed Fermi surface [19, 20], except that semiclassical intuitions based on the effective-mass picture are misleading. We have presented three distinct lines of evidence in support of that view.

We can account for the observed incommensurate collinear magnetic responses as the free responses of the arc metal, after it has gone through a magnetic transition via a central peak mechanism. The doping and temperature trends in the Hall conductivity of the arc metal closely conform to experiment with the single extraneous assumption, that the overall spectral weight is experimentally reduced due to localized states. The non-rigid-band FS evolution with doping is understood through Coulomb effects of the dopants on the orbital splittings in the plane. Finally, the comparatively small Luttinger-sum violations are a direct consequence of the on-site repulsion visible at the Fermi level itself, but as an overall (bulk) effect do not invalidate the quasiparticle picture of the carriers, although their spectral weight is significantly reduced.

Our point of view has received additional experimental support at this conference. The identification of the central peak in the magnetic response [11] has been discussed above. The extension of the SC region to zero doping in PLCCO upon transformation from the T to the T' lattice [21], similar to the one in NCCO thin films [22], is consistent with our understanding of the effects of out-of-plane dopant ions. We concur [21] that the removal of the apical oxygens has caused a strong reduction of the in-plane copper-oxygen splitting. Subsequent charge redistribution between cuppers and oxygens eliminates superexchange, which requires the oxygens to be empty, so that static AF disappears.

An essential ingredient of the picture we draw of all the cuprates is to distinguish copper and oxygen sites. Their relative roles in the SC response remain to be elucidated. A prerequisite for such a step is the proper disentanglement of low energy magnetic and high energy Coulomb effects, which was the principal theme of the present work, and could only be accomplished in a multi-band setting.

## Acknowledgments

Conversations with J. Tranquada and source files of published data provided by A. Fujimori are gratefully acknowledged. This work was supported by the Croatian Government under Project No. 119-1191458-0512.

---

[1] A. T. Bollinger, G. Dubuis, J. Yoon, D. Pavuna, J. Misewich, and I. Bozovic, *Nature* **472**, 458 (2011).  
[2] W. S. Lee, S. Johnston, T. P. Devereaux, and Z.-X. Shen, *Phys. Rev. B* **75**, 195116 (2007).  
[3] D. Reznik, P. Bourges, L. Pintschovius, Y. Endoh, Y. Sidis, T. Masui, and S. Tajima, *Phys. Rev. Lett.* **93**, 207003 (2004).  
[4] S. R. Dunsiger, Y. Zhao, B. D. Gaulin, Y. Qiu, P. Bourges, Y. Sidis, J. R. D. Copley, A. Kallin, E. M. Mazurek, and H. A. Dabkowska, *Phys. Rev. B* **78**, 092507 (2008).  
[5] M. Enoki, M. Fujita, T. Nishizaki, S. Iikubo, D. K. Singh, S. Chang, J. M. Tranquada, and K. Yamada, *Phys. Rev. Lett.* **110**, 017004 (2013).

- [6] Qimiao Si, Yuyao Zha, K. Levin, and J. P. Lu, Phys. Rev. B **47**, 9055 (1993).
- [7] R. S. Markiewicz, J. Lorenzana, G. Seibold, and A. Bansil, Phys. Rev. B **81**, 014509 (2010).
- [8] O. S. Barišić and S. Barišić, J. Supercond. Nov. Magn. **25**, 669 (2012), and references therein.
- [9] Y.-J. Kao, Q. Si, and K. Levin, Phys. Rev. B **61**, R11898 (2000).
- [10] H. J. Schulz, Phys. Rev. Lett. **64**, 1445 (1990).
- [11] Z. J. Xu, C. Stock, S. X. Chi, A. I. Kolesnikov, G. Y. Xu, G. D. Gu, and J. M. Tranquada (2013), manuscript in preparation.
- [12] J. Chang, A. P. Schnyder, R. Gilardi, H. M. Rønnow, S. Pailhes, N. B. Christensen, C. Niedermayer, D. F. McMorrow, A. Hiess, A. Stunault, et al., Phys. Rev. Lett. **98**, 077004 (2007).
- [13] L. P. Gor'kov and G. B. Teitelbaum, Phys. Rev. Lett. **97**, 247003 (2006).
- [14] I. Kupčić and S. Barišić, Phys. Rev. B **75**, 094508 (2007).
- [15] S. Ono, S. Komiya, and Y. Ando, Phys. Rev. B **75**, 024515 (2007).
- [16] S. Mazumdar, in *Interacting electrons in reduced dimensions*, edited by D. Baeriswyl and D. K. Campbell (Plenum Press, New York, 1989), pp. 315–329.
- [17] E. Pavarini, I. Dasgupta, T. Saha-Dasgupta, O. Jepsen, and O. K. Andersen, Phys. Rev. Lett. **87**, 047003 (2001).
- [18] M. Hashimoto, T. Yoshida, H. Yagi, M. Takizawa, A. Fujimori, M. Kubota, K. Ono, K. Tanaka, D. H. Lu, Z.-X. Shen, et al., Phys. Rev. B **77**, 094516 (2008).
- [19] S. I. Mirzaei, D. Stricker, J. N. Hancock, C. Berthod, A. Georges, E. van Heumen, M. K. Chan, X. Zhao, Y. Li, M. Greven, et al., Proceedings of the National Academy of Sciences **110**, 5774 (2013).
- [20] N. Doiron-Leyraud, S. Lepault, O. Cyr-Choinière, B. Vignolle, G. Grissonnanche, F. Laliberté, J. Chang, N. Barišić, M. K. Chan, L. Ji, et al., Phys. Rev. X **3**, 021019 (2013).
- [21] T. Adachi, Y. Mori, A. Takahashi, M. Kato, T. Nishizaki, T. Sasaki, N. Kobayashi, and Y. Koike, Journal of the Physical Society of Japan **82**, 063713 (2013).
- [22] A. Tsukada, Y. Krockenberger, M. Noda, H. Yamamoto, D. Manske, L. Alff, and M. Naito, Solid State Communications **133**, 427 (2005), ISSN 0038-1098.